Earthquakes and Structures, *Vol. 13, No. 2 (2017) 137-150*
DOI: https://doi.org/10.12989/eas.2017.13.2.137

Assessment of post-earthquake serviceability for steel arch bridges with seismic dampers considering mainshock-aftershock sequences

Ran Li[1], Hanbin Ge[*2] and Rikuya Maruyama[2]

[1]*School of Civil Engineering, Southeast University, 2 Sipailou, Xuanwu District, Nanjing, 210096, China*
(Former Visiting Scholar, Meijo University, Nagoya, Japan)
[2]*Department of Civil Engineering, Meijo University, 1-501 Shiogamaguchi, Tempaku-ku, Nagoya, 464-8502, Japan*

(Received April 4, 2016, Revised February 17, 2017, Accepted August 3, 2017)

Abstract. This paper focuses on the post-earthquake serviceability of steel arch bridges installed with three types of seismic dampers suffered mainshock-aftershock sequences. Two post-earthquake serviceability verification methods for the steel arch bridges are compared. The energy-absorbing properties of three types of seismic dampers, including the buckling restrained brace, the shear panel damper and the shape memory alloy damper, are investigated under major earthquakes. Repeated earthquakes are applied to the steel arch bridges to examine the influence of the aftershocks to the structures with and without dampers. The relative displacement is proposed for the horizontal transverse components in such complicated structures. Results indicate that the strain-based verification method is more conservative than the displacement-base verification method in evaluating the post-earthquake serviceability of structures and the seismic performance of the retrofitted structure is significantly improved.

Keywords: post-earthquake serviceability; seismic damper; steel arch bridge; displacement-based verification method; strain-based verification method; seismic performance

1. Introduction

Earthquake disaster is an unexpected disaster which can lead to huge casualties and property damages in a short time. Structures, roads, ports, bridges and dams could be destroyed sometimes accompanying landslides, debris flows, and tsunamis. More seriously, the whole city might be ruined.

Aftershocks are dangerous because they are usually unpredictable, can be of a large magnitude, and can collapse structures that are damaged from the mainshock. (Song *et al*. 2013). Focusing on the destructive earthquakes in recent years, such as Sichuan, China (2008), Papua, Indonesia (2009), Haiti (2010), Chile (2010), Tohoku, Japan (2011), Sichuan, China (2013), Chile (2014) and the latest one in Nepal (2015), the strong aftershocks occurred frequently with high seismic energy follow the mainshocks. For example, in the Japan Tohoku earthquake (USGS 2011) suffered in 2011, about 900 times aftershocks with about 60 aftershocks being over magnitude 6.0 and three over magnitude 7.0 following the mainshock. Though the magnitudes of the aftershocks are usually less than the mainshocks, the peak ground accelerations (PGAs) caused by the aftershocks sometimes are very high or even higher than the mainshocks. The PGA of the October 2004 Mid Niigata Prefecture earthquake recorded at the same station caused by the aftershock was greater than that caused by the mainshock (Kim and Atsumasa 2005, Li *et al*. 2014, NIED 2004). The PGA of the 22 February 2011 Christchurch earthquake reached up to 2.2 g which was the highest recorded in the New Zealand earthquake (Kaiser *et al*. 2012, Potter *et al*. 2015). The Christchurch earthquake is an aftershock of the M7.1 mainshock happened in the Canterbury Plains of New Zealand on 4 September 2010.

The aftershocks might cause severe damage to structures and threaten life safety especially for those structures with deteriorated or degraded performance level. In the 1999 Chi-Chi earthquake, Taiwan, the canopy of a gasoline station was damaged in the mainshock, and later collapsed during an aftershock (Lew *et al*. 2000). The M6.3 Christchurch earthquake five months after the M7.1 mainshock happened in the Canterbury Plains of New Zealand on 4 September 2010 resulted in 185 deaths and approximately US$15 billion rebuild costs (Potter *et al*. 2015, Parker and Steenkamp 2012).

Several detecting and repairing problems have been exposed since the two ruinous earthquakes in Northridge, California (1994), and Hyogoken-Nanbu, Japan (1995), such as the cost of the time and money in identifying and evaluating of structures, the rare possibility to remove damaged structures and rebuild a new one in a short time, and the high cost to change members out of operation every time since the aftershocks are frequent and sometimes destructive. It is necessary to upgrade the seismic performance and to minimize the residual deformation of structures to solve the above problems. Damage control technology as one of the effective techniques to mitigate earthquake disasters has attracted researchers' eyes.

It has been confirmed by quite a few destructive

∗Corresponding author, Professor
E-mail: gehanbin@meijo-u.ac.jp

ISSN: 2092-7614 (Print), 2092-7622 (Online)

Table 1 Verification methods of seismic performance (partial coefficient γ is omitted)

Performance level (Damage state)			Level 1 (Negligible)	Level 2 (Light)	Level 3 (Moderate)	Level 4 (Severe)
Displacement based	Structural safety	①	$\delta_{\max} \le \delta_u$			
	Post-earthquake serviceability	②	$\delta_R \le h/1000$	$\delta_R \le h/300$	$\delta_R \le h/100$	--
Strain based	Structural safety	①	$\varepsilon_{a)\max} \le \varepsilon_u$			
		③	$CID = \sum_{i=1}^{n} \lvert \varepsilon_{pi} \rvert \le CID_{\lim}$			
	Post-earthquake serviceability	②	$\varepsilon_{a)\max} \le \varepsilon_y$	$\varepsilon_{a)\max} \le 2\varepsilon_y$	$\varepsilon_{a)\max} \le 8\varepsilon_y$	--

Note: ①=deformation properties, ②=function maintenance and recovery efficiency, ③=low cycle fatigue, $\delta_{\max}$ =maximum displacement, δ_u =ultimate displacement, δ_R =residual displacement, h = height of bridge pier, CID =cumulative inelastic deformation, ε_{pi} =plastic strain, ε_y =yield strain

earthquakes that the energy dissipation system can cut down the seismic response of structures both in horizontal and vertical directions by increasing the structural damping. In general, a favorable energy dissipation system should have good dissipation capacity to reduce seismic demand on structures and high low-cycle fatigue performance under cyclic loading to resist frequent aftershocks (Li *et al*. 2016).

Kelly *et al*. (1972) and Skinner *et al*. (1975) put forward several types of energy dissipation devices using metallic hysteretic property in the early 1970s. Then they were further developed by many researchers like Usami *et al*. (2004), Honjo *et al*. (2009), Tsai *et al*. (2014). Some devices such as buckling-restrained braces (BRBs) (e.g., Usami *et al*. 2009, Chen *et al*. 2011, Pan *et al*. 2016), shear panel dampers (SPDs) (Ge *et al*. 2011), and shape memory alloy dampers (SMADs) (Luo *et al*. 2009), steel dual-core self-centering braces (SCBs) (Chou *et al*. 2014), were investigated through experimental and simulative methods.

So far, both experimental and analytical studies on energy absorbing capacities of various dampers were also conducted, indicating that an apparent effect on mitigating seismic response of structures was achieved (Koike *et al*. 2008, Usami and Sato 2010, Ge *et al*. 2010). In order to evaluate the post-earthquake serviceability of the structures, the seismic performance verification methods named strain-based verification method and displacement-based verification method have been proposed for the structures which might experience multiple earthquakes in their service life. The methods were recommended by the design guidelines for steel bridges under seismic loading (Usami 2006, JSCE 2008, Usami and Ge 2009) and the Japanese specification for highway bridges (JRA 2012), respectively. In Japan, the two verification methods specified the limit values to different performance levels for bare steel bridges. The seismic performance verification methods have great importance for the structures which might experience multiple earthquakes in their service life. However, for the structural post-earthquake serviceability, the applicability of the two methods to steel bridges installed with dampers has seldom been studied.

In this paper, the post-earthquake serviceability of steel arch bridges is discussed, based on the analytical results of the bare arch bridges and the ones with different types of dampers installed. To investigate the influence of the strong aftershocks, dynamic analyses under a sequence of three earthquake ground motions are carried out to obtain the responses of the steel arch bridges. Correlations between the maximum response displacement and the maximum response strain, the maximum response strain and the residual displacement are investigated. In order to compare the seismic properties of the bridges with different seismic dampers to the one without seismic damper, strain responses at the base of the side piers, displacement responses at the middle point of the girders and the arch ribs of the steel arch bridge are investigated. The residual displacements in special positions are also drawn. Then, the strain-based verification method is adopted to estimate the post-earthquake serviceability of the structures with seismic dampers. Moreover, based on these results, the consistence of the two verification methods in evaluating the post-earthquake serviceability of structures is elucidated.

2. Post-earthquake serviceability verification methods

The displacement-based verification method is straightforward and correlated with ductility design, which has long been conceptually accepted (e.g., Chen *et al*. 2007). The strain-based verification method as a dynamic verification method has been discussed and validated for steel bridge piers and single-deck portal frame piers (e.g., Morishita *et al*. 2002). In this study, the performance levels of the steel members are evaluated using the displacement-based and the strain-based verification methods, respectively.

In the earthquake engineering, four performance levels which correspond to different damage states (negligible,

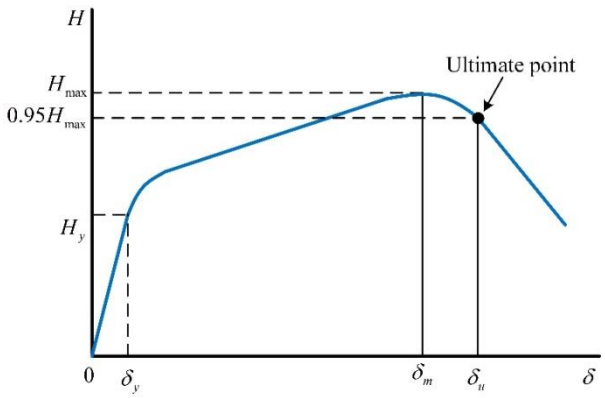

Fig. 1 Envelop of load-displacement hysteretic curve of structures

light, moderate, and severe) are commonly used. Table 1 shows the four performance levels given in Japanese guidelines (Usami 2006, JSCE 2008, Usami and Ge 2009) of the two verification methods in detail. For the displacement-based verification method, the residual displacements, δ_R, of the level 1, level 2 and level 3 should not exceed $h/1000$, $h/300$ and $h/100$, respectively. For the strain-based verification method, the average compressive strains $\varepsilon_{a)\max}$ of the level 1, level 2 and level 3 should respectively satisfy $\varepsilon_{a)\max} \le \varepsilon_y$, $\varepsilon_{a)\max} \le 2\varepsilon_y$ and $\varepsilon_{a)\max} \le 8\varepsilon_y$ at the critical segments of the bridge. The damage level is classified to performance level 4 when the residual displacements δ_R exceeds $h/100$ for the displacement-based verification method and the average maximum strain $\varepsilon_{a)\max}$ exceeds $8\varepsilon_y$ for the strain-based verification method, respectively.

It should be noted that both the ultimate displacement and ultimate strain in Table 1 are at the instant when the strength decreases to 95% of the peak load in a horizontal load-displacement curve (Zheng *et al*. 2000, Usami 2006, Usami and Ge 2009). The load-displacement curve is depicted in Fig. 1, in which the ultimate point is plotted. The maximum strain $\varepsilon_{a)\max}$ is defined as the average value of the maximum compressive strains within critical segments (Zheng *et al*. 2000).

In this study, one target of the post-earthquake serviceability of the structures encountered mainshock-aftershocks sequence is to satisfy the performance level 2. Performance level 2 corresponds to slight damage of structural members or components, where the strength decrease in the plastic deformation is very small, and members can function after simple retrofitting. The requirements according to the displacement-based and strain-based verification methods are respectively given in Eqs. (1)-(2)

$$\delta_R \le h/300 \tag{1}$$

$$\varepsilon_{a)\max} \le 2\varepsilon_y \tag{2}$$

The second purpose is to confirm the relationship of the two methods in verifying the post-earthquake performance of structures installed with three types of seismic dampers.

3. Seismic analysis

3.1 Background of steel arch bridge

The target bridge as shown in Fig. 2 is a reinforced concrete (RC) upper-deck arch bridge, which is specified as a benchmark model for seismic evaluation by Japan Society

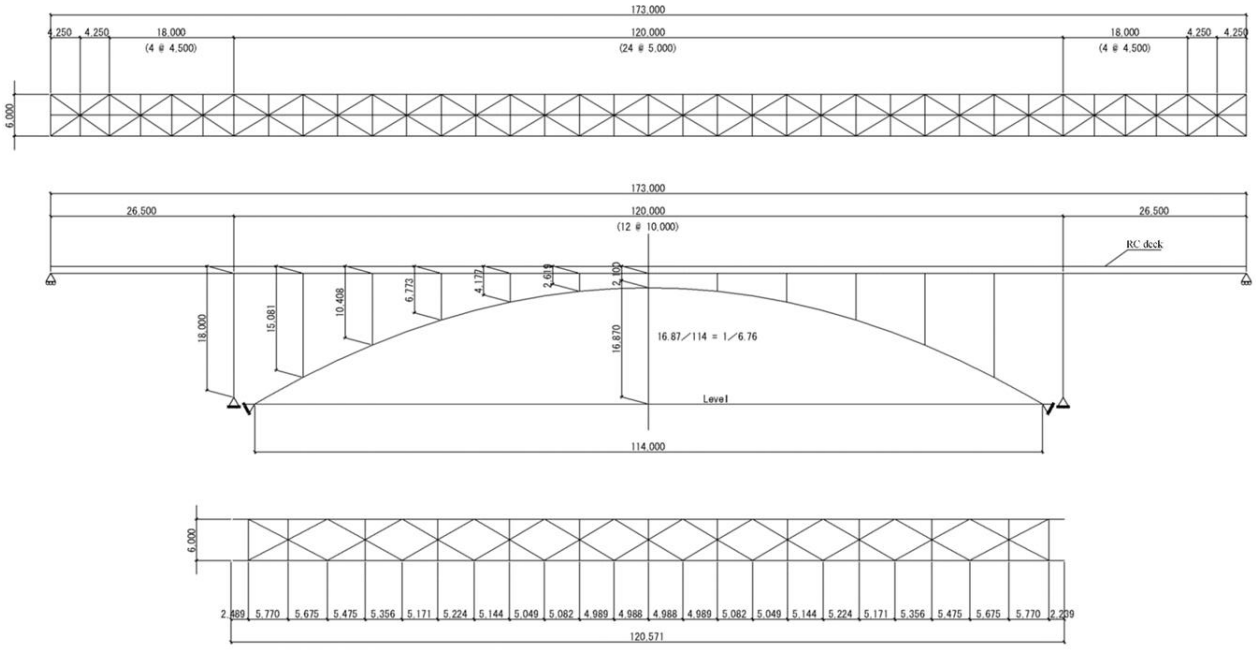

Fig. 2 Schematic figure of steel arch bridge

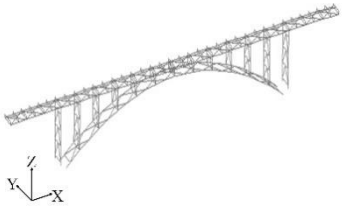

(a) Original model (OM)

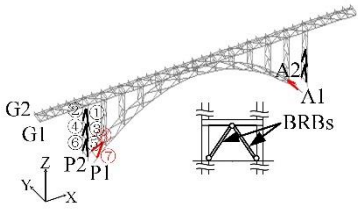

(b) Seismic upgrading model 1 (UM_1, Type I)

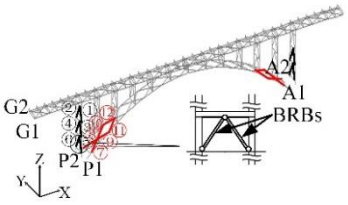

(c) Seismic upgrading model 1 (UM_1, Type II)

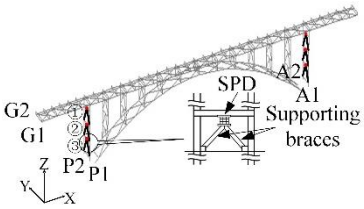

(d) Seismic upgrading model 2 (UM_2)

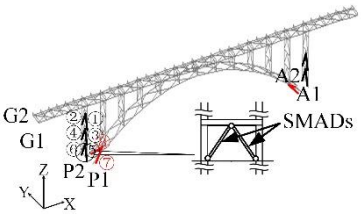

(e) Seismic upgrading model 3 (UM_3, Type I)

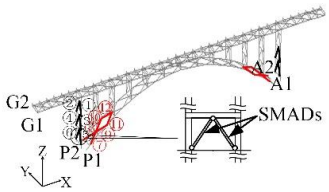

(f) Seismic upgrading model 3 (UM_3, Type II)

Fig. 3 Analytical models used in the analysis of steel arch bridges

of Steel Construction (JSSC) (Usami 2002, 2003). This bridge was designed only considering the moderate (level 1) earthquake in accordance with the specifications for highway bridges (JRA 1996, 2002). This bridge, with a total length of 173 m as shown in Fig. 2, is symmetrical with respect to the longitudinal and perpendicular axes. A hinged steel arch has a span of 114 m and a rise at the crown of 16.87 m, with a rise-span ratio of 1/6.76. There are also two side spans of 26.5 m at both ends of the steel arch.

3.2 Analytical model of steel arch bridge

In this section, the properties of the model in the transverse direction are considered. The 3D configuration of the bridge without dampers, named the original steel arch bridge model, OM, is given in Fig. 3(a). Figs. 3(b)-(f) present the three types of retrofitted models called seismic upgrading models. The earthquake ground motions in Japan are divided into two categories, i.e., Type I and Type II. Type I earthquake is the marine type earthquake with large amplitude and long duration repeated action, and Type II earthquake is the near field type with strong accelerations and short duration. The intensities of the Type I and Type II seismic waves are 1000 gal and 2000 gal for the Level 2 earthquake, respectively. For the two different types of ground motions, two corresponding retrofitting plans using the BRBs are shown in Figs. 3(b)-(c). The upgrading model using the BRBs is denoted by UM_1, and the BRBs with different number are installed at both the side columns and arch ribs based on different ground motions. The second upgrading model, UM_2, illustrated in Fig. 3(d), is retrofitted using the SPDs only in the side columns, which is different from UM_1. The third upgrading model, UM_3, illustrated in Figs. 3(e)-(f), is similar to that of UM_1, where the BRBs are replaced by the SMADs.

Element types and steel grades of the arch bridge are presented in Table 2. In the analytical model, three-dimensional (3D) Timoshenko beam element, B31 with the shear deformation considered is used to model the deck slabs, girders, columns, arch ribs, and transverse bracings. For this bridge, the slenderness ratios of the diagonal braces are large, and the rotational stiffness of the connection has minor effect on the internal forces of the braces. Hence, the diagonal braces can be modeled as truss elements. 3D truss element, T3D2, is employed for the diagonal braces.

In addition, a bilinear kinematic hardening model, shown in Fig. 4(a), with the elastic modulus $E = 206\,\text{GPa}$ and the strain-hardening modulus $E' = E/100$ (Lu *et al*. 2004, Usami *et al*. 2004), is applied to the steel. Fig. 4(b) gives the stress-strain relationship for the RC deck provided by the specification for highway bridges (JRA 2012) with a compressive strength $f_c = 0.85\sigma_{ck}$, design strength $\sigma_{ck} = 30\,\text{MPa}$ and ultimate compressive strain $\varepsilon_0 = 0.002$. However, the tensile strength of the concrete is neglected in this model. Furthermore, geometrical nonlinearity is taken into account in the dynamic analysis.

In the seismic design of the UM_1 with the BRBs, the UM_2 with the SPDs, and the UM_3 with the SMADs, level 1 seismic waves for the ground motions of Type 1 are employed for the primary design. All the members of the arch bridges are designed to be elastic in the primary design. The design methods of the BRBs, SPDs and

Table 2 Element type and steel grade of steel arch bridge member

Bridge member	Element type	Steel grade
Side pier, girder, arch rib	Beam	SMA490
Vertical member, deck slab, supporting of arch rib		SMA400
Diagonal brace	Truss	SMA490
Transverse member		

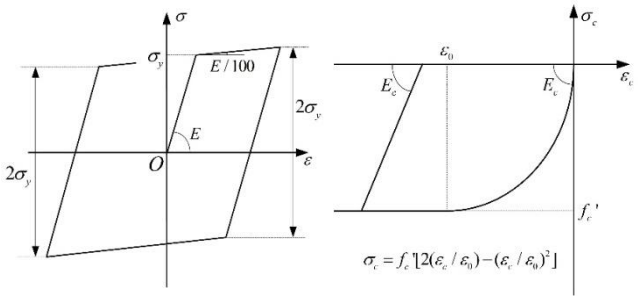

(a) Stress-strain relation of steel (b) Stress-strain relation of concrete

Fig. 4 Constitutive models for steel arch bridges

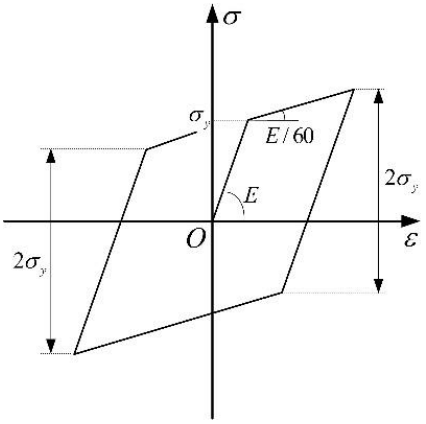

(a) Bilinear kinematic hardening model (BRB)

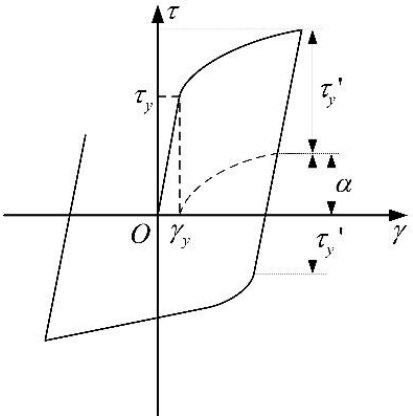

(b) Combined hardening model (SPD)

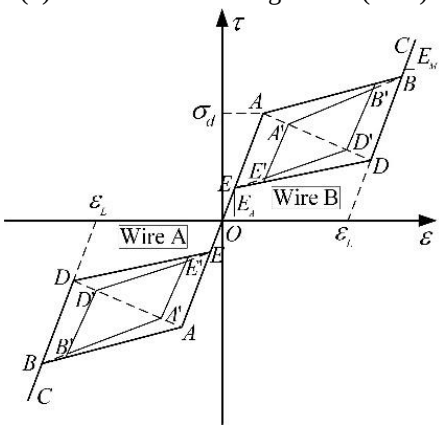

(c) Multi-linear model (SMAD)

Fig. 5 Constitutive models of seismic dampers for steel arch bridges

Table 3 Section area of BRBs installed in steel arch bridges

BRB in Arch	Ground type	Position of BRB	A_{BRB} (mm^2)
Upgrading arch model 1	I	Side pier	3000
		Arch rib ⑦,⑧	8500
	II	Side pier	5000
		Arch rib ⑦,⑧	10000
		Arch rib ⑨~⑫	5500

Table 4 Parameters of SPDs installed in steel arch bridges

SPD in Arch	α_F	$a = b_w$ (mm)	t_w (mm)	$H_{y,SPD}$ (kN)	K_{SPD} (×10^6 kN/m)
Upgrading arch model 2	0.2	500	19.80	1343	1.57
		600	16.50		1.31
		700	14.14		1.12
		800	12.38		0.98
		900	11.00		0.87
		1000	9.90		0.78

Note: α_F=ratio of yield strength, a=panel width, b_w=panel height, t_w=web thickness, K_{SPD}= stiffness

Table 5 Section area of SMADs installed in steel arch bridges

SMAD in Arch	Ground type	Position of SMA	A_{SMAD} (mm^2)
Upgrading arch model 3	I	Side pier	600
		Arch rib ⑦,⑧	1700
	II	Side pier	2500
		Arch rib ⑦,⑧	5000
		Arch rib ⑨~⑫	2750

SMADs have been introduced by Li *et al*. (2016). The constitutive models of BRBs, SPDs and SMADs used in this section are shown in Figs. 5(a)-(c), respectively. For the UM_2, 6 different values are specified for the height of shear panel $b_w = 0.5 \sim 1.0\text{m}$ and a constant value of 0.2 is given to yield strength factor α_F=0.2. Parameters of the BRBs, the SPDs and the SMADs are presented in Tables 3-5, respectively.

The ground motions employed in the analyses are presented with the maximum acceleration in Table 6. A number of analyses have been carried out on frame-type bridge piers with seismic dampers in one of the authors' group (e.g., Chen *et al*. 2007, 2008, Luo *et al*. 2009, Ge *et al*. 2011), where 3 representative seismic waves had been employed. In this study, 12 waves including the 3 representative waves were selected for the arch bridges with the BRBs and SPDs based on the previous studies. Totally time-history analyses on 36 cases (each of the 12 ground motions repeated for one time, two times, and three times) were carried out for the bare arch. Two upgrading approaches are employed for the arch bridge with the BRBs, each with 18 cases, where the total cases are 36. However, in the arch bridge with the SMADs, 6 ground

Table 6 Ground motion and the abbreviation of different models

Ground motion (Level 2, Type 1)	Abbreviation	Input model				Maximum acceleration (gal (cm/s^2)
		OM	BRB	SPD	SMAD	
Kaihoku Bridge (Longitudinal)	KAI-LG-M	$O^{1,2,3}$	$O^{1,2,3}$	$O^{1,2,3}$	$O^{1,2,3}$	318.8
Kaihoku Bridge (Transverse)	KAI-TR-M	$O^{1,2,3}$	$O^{1,2,3}$	$O^{1,2,3}$	$O^{1,2,3}$	346.4
Shichimine Bridge (Longitudinal)	SHI-LG-M	$O^{1,2,3}$	$O^{1,2,3}$	$O^{1,2,3}$	$O^{1,2,3}$	319.6
Itabashima Bridge (Longitudinal)	ITA-LG-M	$O^{1,2,3}$	$O^{1,2,3}$	$O^{1,2,3}$	O^{1}	346.0
Itabashima Bridge (Transverse)	ITA-TR-M	$O^{1,2,3}$	$O^{1,2,3}$	$O^{1,2,3}$	--	384.9
Onnetou Bridge (Transverse)	ONN-TR-M	$O^{1,2,3}$	$O^{1,2,3}$	$O^{1,2,3}$	O^{1}	345.5
Ground motion (Level 2, Type 2)	Abbreviation	Input model				Maximum acceleration (gal (cm/s^2))
		OM	BRB	SPD	SMAD	
JMAObservatory (NS)	JMA-NS-M	$O^{1,2,3}$	$O^{1,2,3}$	$O^{1,2,3}$	$O^{1,2,3}$	588.1
JMA Observatory (EW)	JMA-EW-M	$O^{1,2,3}$	$O^{1,2,3}$	$O^{1,2,3}$	$O^{1,2,3}$	765.9
Inagawa Bridge (NS)	INA-NS-M	$O^{1,2,3}$	$O^{1,2,3}$	$O^{1,2,3}$	$O^{1,2,3}$	780.0
JR Takatori Station (NS)	JRT-NS-M	$O^{1,2,3}$	$O^{1,2,3}$	$O^{1,2,3}$	--	686.8
JR Takatori Station (EW)	JRT-EW-M	$O^{1,2,3}$	$O^{1,2,3}$	$O^{1,2,3}$	O^{1}	654.8
Fukiai Supply Station Osaka Gas Corp. (N27W)	FUKIAI-M	$O^{1,2,3}$	$O^{1,2,3}$	$O^{1,2,3}$	O^{1}	736.3

Note: Figures in the upper right corner of the circles are the number of input ground motions.

Table 7 Eigenvalue analysis results of steel arch bridges

Model	Mode	Natural period T (s)	Effective mass ratio (%)			Deformation mode
			Longitudinal	Transverse	Vertical	
OM	1	1.32	14.8	0	0	In-plane
	2	1.02	0	73.6	0	Out-of-plane
UM_1	1	1.32	16.4	0	0	In-plane
	2	1.13	0	85.8	0	Out-of-plane
UM_2	1	1.32	16.2	0	0	In-plane
	2	0.99	0	80.8	0	Out-of-plane
UM_3	1	1.53 (1.59)	16.4	0	0	In-plane
	2	1.32	0	90.6 (90.1)	0	Out-of-plane

Note: Modes of UM_1 in two ground types are the same, they are thus merged in the table, and numbers in the brackets are the mode of Ground type II of UM_3

motions are repeated for three times to simulate the mainshock-aftershock sequences except for 4 seismic waves. The reason is due to difficulties in the convergence of analyses with the user-defined subroutines for the SMA and the concrete. For the arch bridge with the SPDs, totally 216 cases were studied, with a constant α_F and 6 values for α_K under the 36 seismic waves based on the former study of the authors' group. In total, 310 cases were analyzed for the bare arch bridges and the ones with the dampers.

3.3 Analysis results

3.3.1 Eigenvalue analysis results

Eigenvalue analyses are conducted to obtain a fundamental insight into dynamic characteristics of the four models. Results of the eigenvalue analyses are listed in Table 7. For the longitudinal direction, the results indicate that the first order natural periods of the first three models (OM, UM_1, UM_2) are the same. The reason is that both change in the stiffness and the deformation generated in the seismic dampers along the longitudinal direction are negligible. However, the first order natural period of the UM_3 with the SMADs, is elongated obviously due to the weakened stiffness in the longitudinal direction, and the effective mass ratio of mode 1 is increased from 73.6% to 90.6%, compared with that of the bare arch bridge. For the second eigenvalue, the differences in the natural periods could attribute to the different transverse stiffness of the models with different dampers.

3.3.2 Transverse residual displacement

In order to determine the focus point in the following analyses, the transverse residual displacement of the bare arch bridge under the ground motion INA-NS-M is investigated. Fig. 6 shows the residual displacement distribution along the length of the members, i.e., girder,

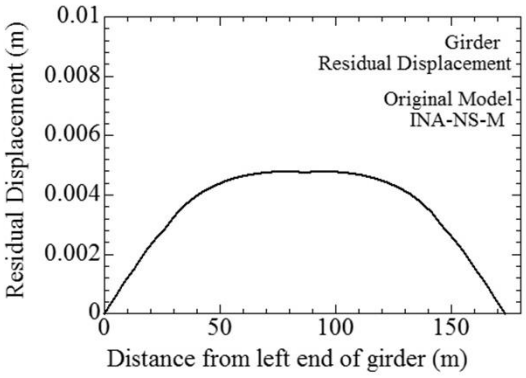

(a) Girder

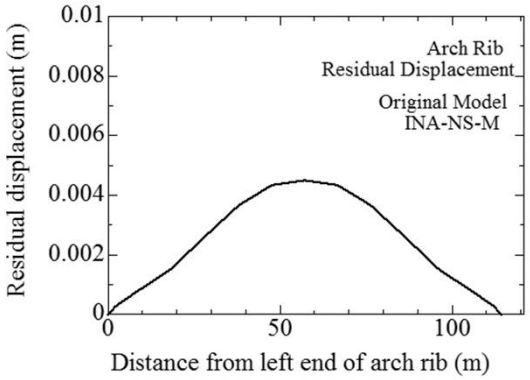

(b) Arch rib

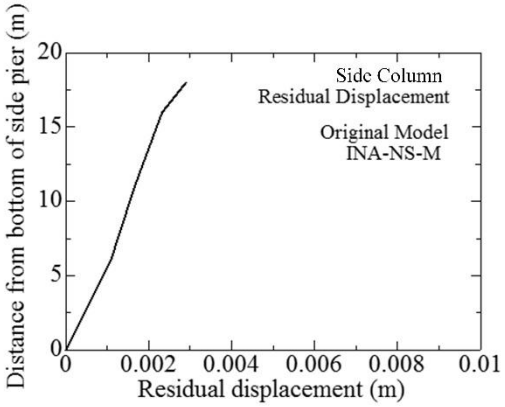

(c) Side column

Fig. 6 Residual displacement of steel arch bridge members in transverse direction

arch rib and side column. The vertical axes of Figs. 6(a)-(b) denote the residual displacements, and the horizontal axes represent the length of the members. Contrarily, the vertical axis in Fig. 6(c) is the height of the side column and the horizontal axis shows the residual displacement. It can be seen from Figs. 6(a)-(b) that the maximum residual displacements of the stiffened girders and the arch ribs appear at the mid span of the members. On the other hand, the maximum residual displacement, shown in Fig. 6(c), occurs at the top of the side column. Therefore, to investigate the correlation between the maximum response strain and the residual displacement of the arch bridge, strains at the bases of the side columns, residual displacements at the mid span of the girders, the arch ribs and the top of the side columns are employed.

3.3.3 Relative residual displacement

Displacement-based verification method for evaluating post-earthquake serviceability has not presented an approach to verify the horizontal members of a structures (JSCE 2008, JRA 2012). In this paper, the relative displacement is taken as the relative residual displacement of a horizontal member, and L_i denotes the distance between two adjacent vertices of a transverse bracing. The definition for relative displacement is illustrated in Fig. 7. The relative displacement, δ_R, is the difference between displacement at point B (δ_B) and that at the reference point A (δ_A). When the

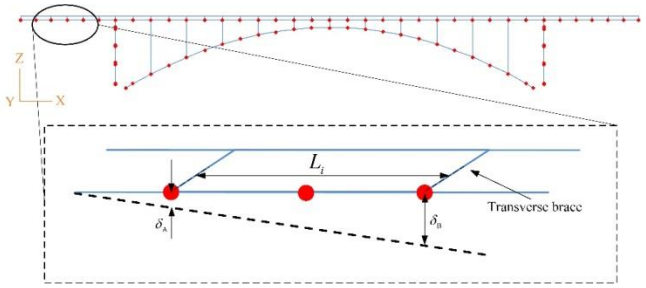

Fig. 7 Definition of relative displacement

displacement-based verification method is employed, Eq. (1) can be used by substituting the height of the pier h, by the horizontal distance of the transverse bracing, L_i. For the strain-based verification method, Eq. (2) can be used directly.

3.3.4 Simulation results

Fig. 8 gives the maximum strain-residual displacement relationship at different locations with the mid span of the girder shown in Fig. 8(a-1), Fig. 8(b-1), the mid span of the arch rib in Fig. 8(a-2), Fig. 8(b-2), and the top of the side column in Fig. 8(a-3), Fig. 8(b-3) of the OM and the UM_1. Fig. 8(a) is the statistic distribution, and Fig. 8(b) is the magnified subset of Fig. 8(a). The digits followed GM (ground motion) mean the repeated times of earthquake excitation. Fig. 8(a) indicate that the bare arch bridges

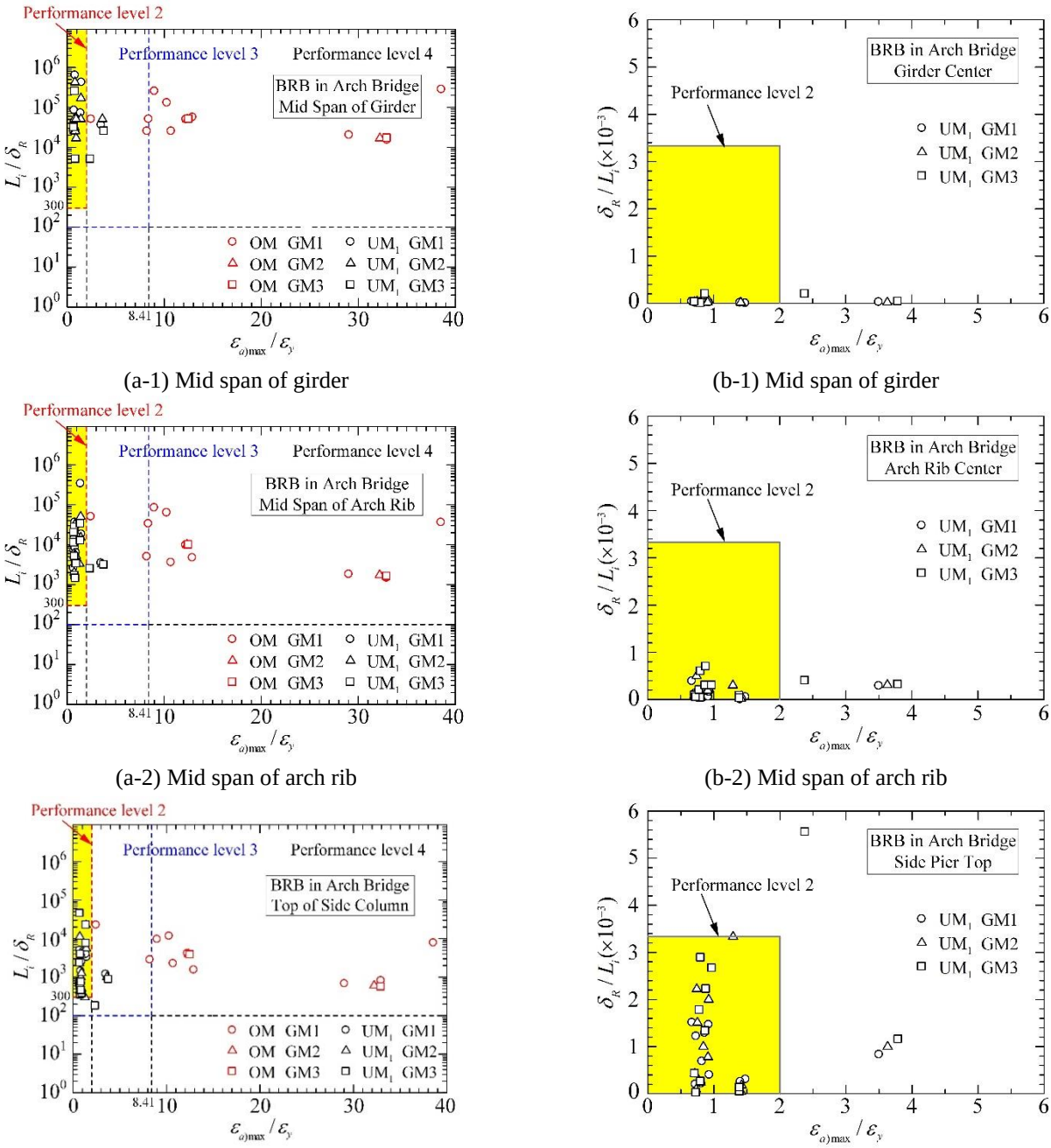

(a-1) Mid span of girder

(b-1) Mid span of girder

(a-2) Mid span of arch rib

(b-2) Mid span of arch rib

(a-3) Top of side column

(b-3) Top of side column

(a) Statistic distributions of maximum strain-residual displacement relation

(b) Magnified subsets of (a)

Fig. 8 Maximum strain-residual displacement relation of different positions of steel arch bridges with and without BRBs

(OM) can generally satisfy the requirement of the performance level 2 according to the displacement-based verification method, but the maximum strains are larger than $2\varepsilon_y$. For the arch bridges installed with the seismic dampers, only 4 cases fail to meet the requirements of the performance level 2 according to the two verification methods. Meanwhile, significant mitigation of the maximum strain and residual displacement are achieved for the arch bridges with the seismic dampers compared with the corresponding bare arch bridges, which can be found in Fig. 8(b).

However, one case marked with a circle with dotted line in Fig. 8(a-3) and Fig. 8(b-3) which is one of the UM_1 under GM3, has not satisfied the performance level 2 of the two methods. Both the residual displacement, δ_R, at the top of the side column and the maximum strain, $\varepsilon_{a)\max}$, at the column base exceed the allowable value, L_i/300 and $2\varepsilon_y$, respectively. This may be because the residual displacement, δ_R, and the maximum strain, $\varepsilon_{a)\max}$, of the bridge with BRBs in this specific ground motion are larger than the others.

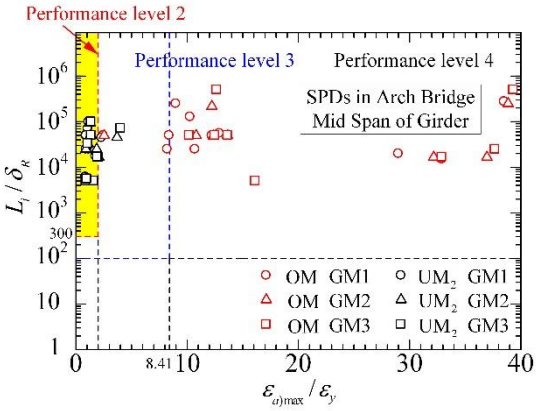

(a-1) Mid span of girder

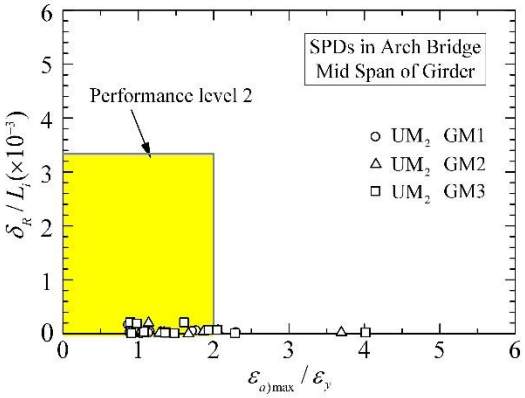

(b-1) Mid span of girder

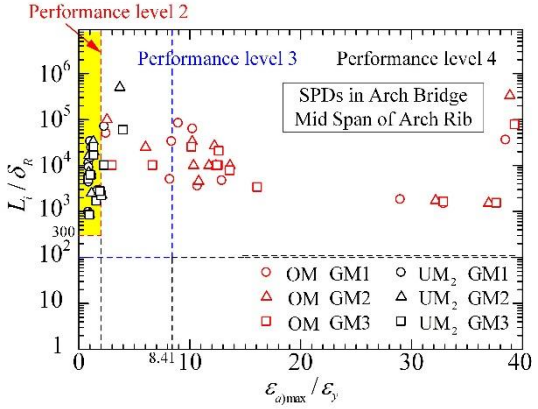

(a-2) Mid span of arch rib

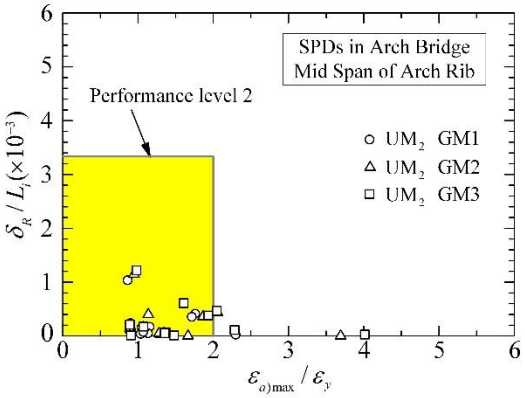

(b-2) Mid span of arch rib

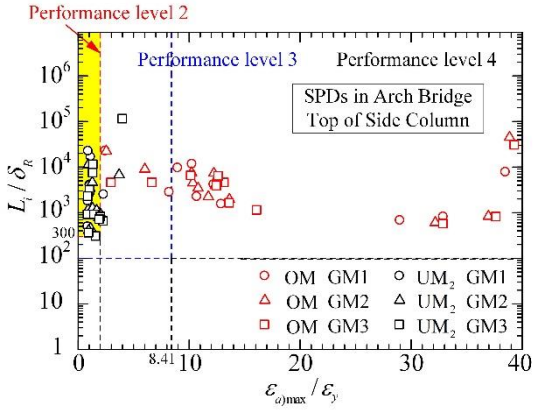

(a-3) Top of side column

(a) Statistic distributions of maximum strain-residual displacement relation

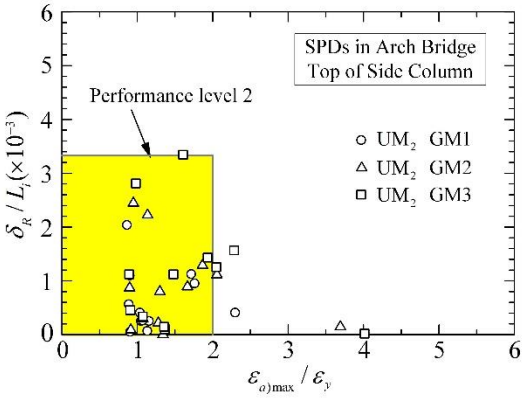

(b-3) Top of side column

(b) Magnified subsets of (a)

Fig. 9 Maximum strain-residual displacement relation of different positions of steel arch bridges with and without SPDs

From the above discussions, the maximum strain of the members can be controlled within $2\varepsilon_y$ based on the seismic design for complicated structures like steel arch bridge with the BRBs employed in this paper.

Figs. 9 and 10 present the analysis results of the upgraded arch bridges with the SPDs and the SMADs, i.e., the UM_2 and the UM_3, respectively. The relationship of the maximum strains at the base of the side columns and the residual displacements at the mid span of the girders are given in Fig. 9(a-1), Fig. 9(b-1) and Fig. 10(a-1), Fig. 10(b-1), that at the mid span of the arch ribs in Fig. 9(a-2), Fig. 9(b-2), Fig. 10(a-2), and Fig. 10(b-2), and that at the top of the side columns is shown in Fig. 9(a-3), Fig. 9(b-3), Fig. 10(a-3) and Fig. 10(b-3). The layout of Figs. 9-10 is the same as that of Fig. 8. The maximum strains and the residual displacements of the arch bridges with the seismic dampers satisfy the requirements of the two verification methods, which is similar to the result of the UM_1. In general, the model with SPDs has the maximum residual displacement among the three updated models. The

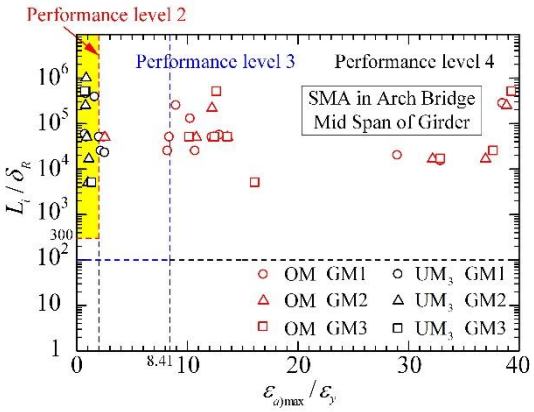

(a-1) Mid span of girder

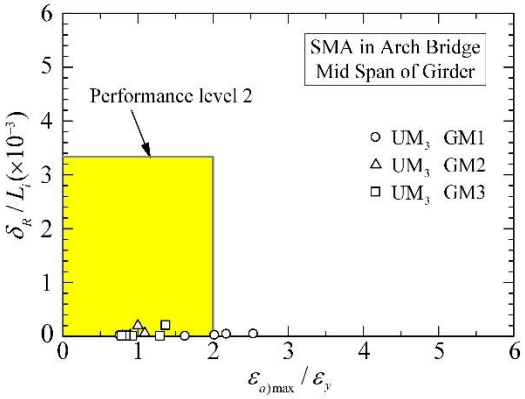

(b-1) Mid span of girder

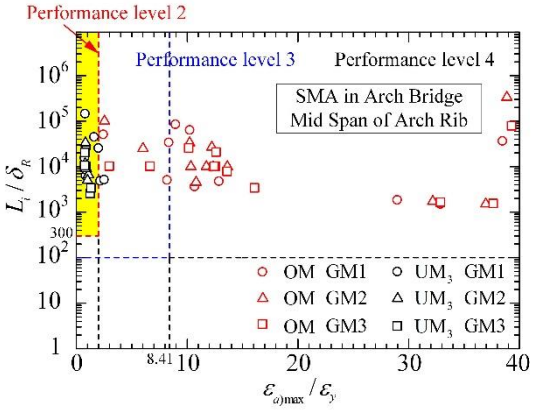

(a-2) Mid span of arch rib

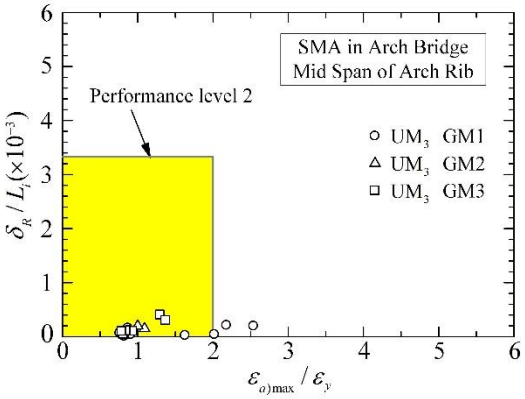

(b-2) Mid span of arch rib

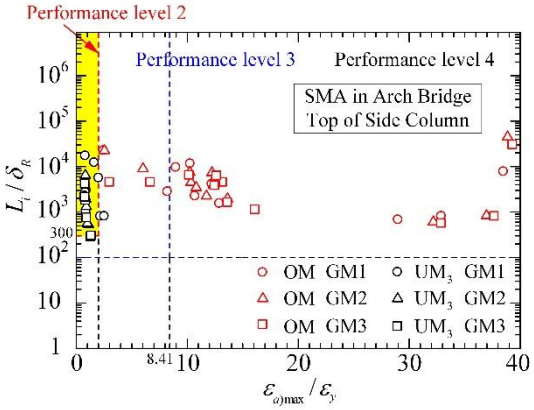

(a-3) Top of side column

(a) Statistic distributions of maximum strain-residual displacement relation

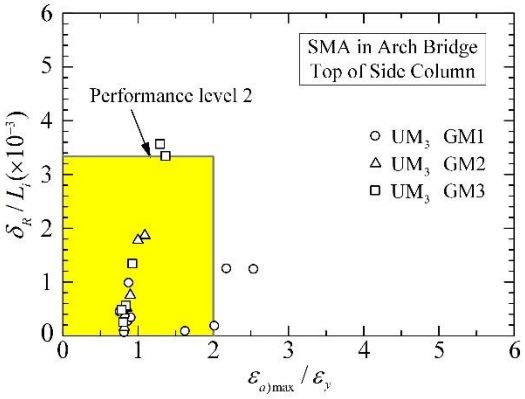

(b-3) Top of side column

(b) Magnified subsets of (a)

Fig. 10 Maximum strain-residual displacement relation of different positions of steel arch bridge with and without SMAD

minimum residual displacement appears at the model with SMADs. The residual displacement of model with BRBs is between those of models with SPDs and SMADs.

To quantitatively evaluate the applicability of the two verification methods to the arch bridge, a new index $\bar{\kappa}$ is defined in Eq. (3)

$$\bar{\kappa} = \frac{\bar{\delta}}{\bar{\varepsilon}} \tag{3}$$

where $\bar{\delta} = \dfrac{\delta_R}{h/300}$, $\bar{\varepsilon} = \dfrac{\varepsilon_{a)\max}}{2\varepsilon_y}$. This index indicates relative evaluation results according to the two verification results, where a value less than 1.0 denotes that evaluation result of the post-earthquake serviceability according to the displacement-based method gives a less critical state, and the strain-based method gives a relatively conservative evaluation result. Mean values $\bar{\kappa}$ and standard deviations of $\bar{\kappa}$ of the members in the bare arch bridges and the

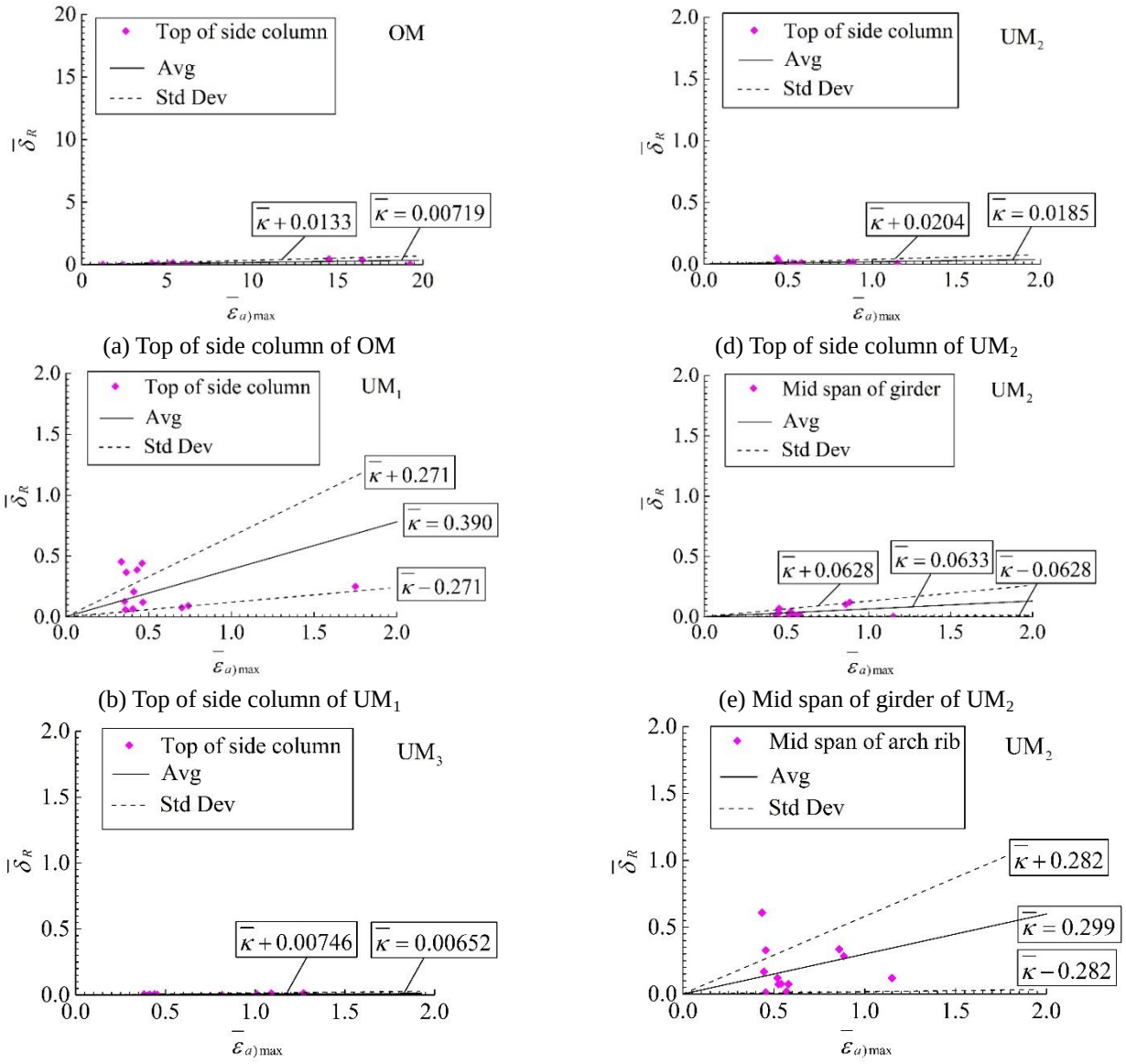

(a) Top of side column of OM

(d) Top of side column of UM_2

(b) Top of side column of UM_1

(e) Mid span of girder of UM_2

(c) Top of side column of UM_3

(f) Mid span of arch rib of UM_2

Fig. 11 Normalized residual displacement and normalized maximum strain relationship with and without dampers in different positions of steel arch bridge

upgraded ones are illustrated in Fig. 11, where the average value at the top of the side column shown in Figs. 11(a)-(d) ranges from 0.00652 to 0.39. Large deviations of $\bar{\kappa}$ are observed for the cases analyzed in the figures. It is also found that $\bar{\kappa}$ is largest at the mid span of the arch rib, as shown in Figs. 11(d)-(f).

The maximum strains at the column bases of the bear arch bridges and the 3 upgrading ones are compared in Fig. 12. The maximum strains of the 3 upgrading arch bridges installed with the seismic dampers are largely reduced, and most of them are all less than $2\varepsilon_y$ except for one case. For the ground motion SHI-LG-M, the maximum strain of the UM_2 exceeds the limit value $2\varepsilon_y$ at the 3rd time excitation. This may be because that the SPDs used in the bridge have a relatively weak seismic effect to this specific ground motion after times excitation.

Fig. 13 shows the residual displacements of the mid span of the girders, the mid span of the arch ribs and the top of the side piers. It is apparent that the residual displacements of the aforementioned locations increase subsequently. In general, UM_1 in Type I motions has a largest value among others. However, it appears dispersion in Type II motions. There might two reasons lead to this phenomenon. On the one hand, it is influenced by the intensities and the durations of different ground type. On the other hand, even for different ground motions of the same ground type, the tendency of the structural responses might be diverging by using different retrofit plans. In other words, different dampers have different sensitivity under different seismic waves for the structural responses. Moreover, for the upgraded arch bridges, the maximum strains of most cases shown in Figs. 12 and 13 are less than $2\varepsilon_y$, and the residual displacements are far less than the limit value, $h/300$.

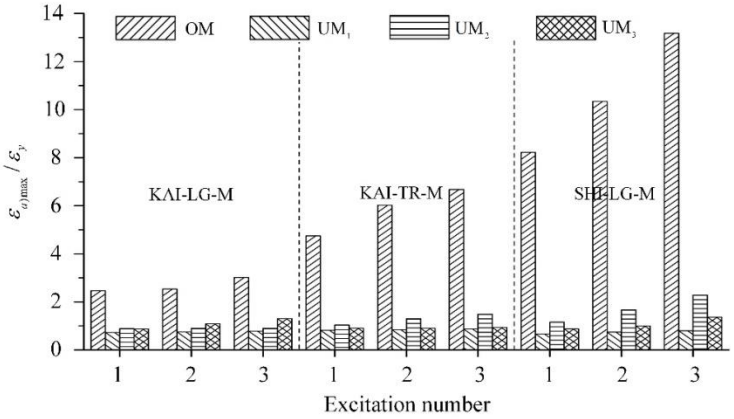

(a) Ground type I

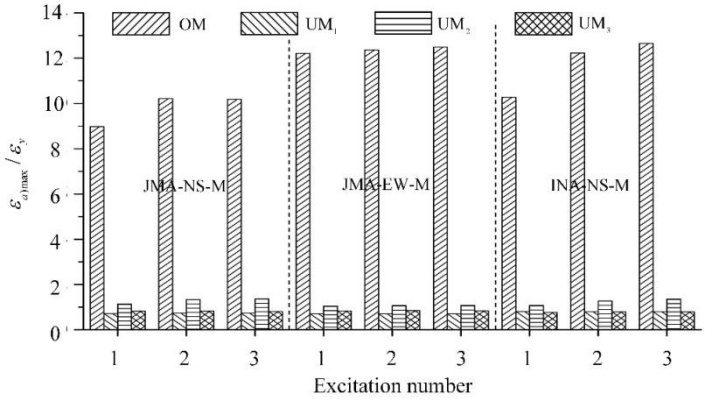

(b) Ground type II

Fig. 12 Maximum strain of different models in different ground motions

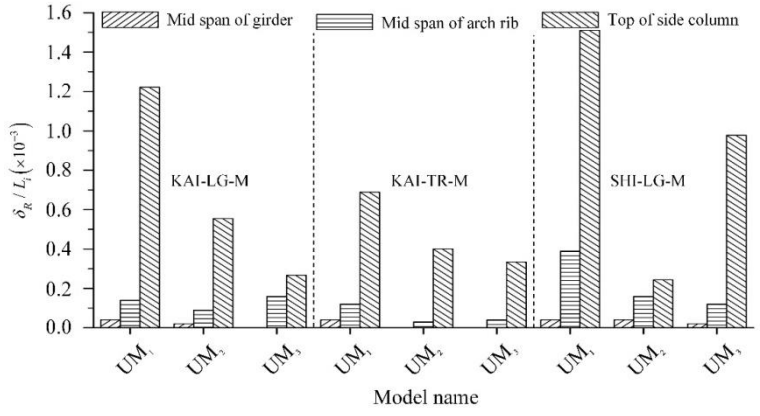

(a) Ground type I

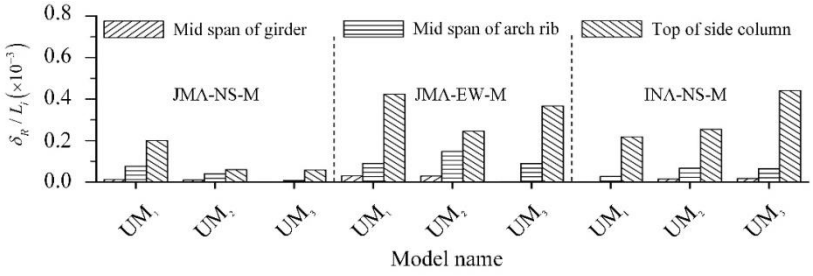

(b) Ground type II

Fig. 13 Residual displacement of different positions of models in different ground motions: (a) Ground type I and (b) Ground type II

From the analyses results of the 3 upgrading arch bridges, it is obvious that the maximum strains are less than the limit value of the strain-based verification method, $2\varepsilon_y$, while the residual displacements are far below the limit value of the displacement-based verification method, h/300. In other words, for the steel arch bridge, the strain-based verification method is more conservative than the displacement-based verification method in the evaluation of the post-earthquake serviceability.

4. Conclusions

In this study, 3 types of seismic dampers are applied to retrofit a benchmark steel arch bridge. Dynamic analyses are carried out to examine the effectiveness of retrofitted structures with the seismic dampers. The performance of the steel arch bridge with seismic dampers under repeated earthquakes is also investigated. Moreover, the post-earthquake serviceability of the structures is verified by both the strain-based and the displacement-based methods. Conclusions are summarized as follows.

1. Damage control effects of the dampers are investigated. It is found that all the dampers can greatly improve the seismic performance of the structures. The control effect of the retrofitted steel arch bridges with SPDs, BRBs and SMADs have a tendency to decline subsequently.
2. The steel arch bridges installed with BRBs, SPDs and SMADs are investigated. The relative displacements of the side columns and, the arch ribs are discussed. The strain-based verification method dominated by the maximum strain $2\varepsilon_y$ can be put into practice for the verification of the post-earthquake serviceability. It is more conservative than the displacement-based verification method.
3. The relative displacement is proposed for the horizontal transverse components. The strain-based verification method also works in the horizontal transverse components.
4. The post-earthquake serviceability of the steel arch bridges is weakened with the increasing number of the aftershock sequence.
5. The post-earthquake serviceability of the structures can be satisfied by reducing the maximum strain and the residual displacement which can be controlled by the number and the install position of BRBs, SPDs or SMADs.

Acknowledgements

The study is supported in part by grants from the Advanced Research Center for Natural Disaster Risk Reduction, Meijo University, which supported by Ministry of Education, Culture, Sports, Science and Technology (MEXT), Japan.

References

Chen, X., Ge, H.B. and Usami, T. (2011), "Seismic demand of buckling-restrained braces installed in steel arch bridges under repeated earthquakes", *J. Earthq. Tsunami*, **5**(2), 119-150.

Chen, Z.Y., Ge, H.B. and Usami, T. (2008), "Analysis and design of steel bridge structures with energy absorption members", *Int. J. Adv. Steel Constr.*, **4**(3), 173-183.

Chen, Z.Y., Ge, H.B., Kasai, A. and Usami, T. (2007), "Simplified seismic design approach for steel portal frame piers with hysteretic dampers", *Earthq. Eng. Struct. D.*, **36**(4), 541-562.

Chou, C.C., Chen Y.C., Pham, D.H. and Truong, V.M. (2014), "Steel braced frames with dual-core SCBs and sandwiched BRBs: Mechanics, modeling and seismic demands", *Eng. Struct.*, **72**, 26-40.

Ge, H.B., Chen, X. and Matsui, N. (2011), "Seismic demand on shear panel dampers installed in steel-framed bridge pier structures", *J. Earthq. Eng.*, **15**(3), 339-361.

Ge, H.B., Kaneko, K. and Usami, T. (2010), "A study on cyclic behavior and hysteretic model of high-performance stiffened shear panel dampers", *J. Struct. Eng.*, JSCE, **56**A, 522-532. (in Japanese)

Honjo, K., Yokoyama, K. Maehara, N., Tasaki, K. and Kawakami, M. (2009), "Seismic retrofitting study of a steel upper-deck type arch bridge", *J. Struct. Eng.*, JSCE, **55**A, 515-524. (in Japanese)

JRA (1996), *Specification for highway bridges, Part V: Seismic design*, Japan Road Association, Tokyo, Japan. (in Japanese)

JRA (2002), *Specification for highway bridges, Part V: Seismic design*, Japan Road Association, Tokyo, Japan. (in Japanese)

JRA (2012), *Specification for highway bridges, Part V: Seismic design*, Japan Road Association, Tokyo, Japan. (in Japanese)

JSCE (2008), *Standard specifications for steel and composite structures, Seismic design*, Japan Society of Civil Engineers, Tokyo, Japan. (in Japanese)

Kaiser, A., Holden, C., Beavan, J., Beetham, D., Benites, R., Celentano, A., Collett, D., Cousins, J., Cubrinovski, M., Dellow, G., Denys, P., Fielding, E., Fry, B., Gerstenberger, M., Langridge, R., Massey, C., Motagh, M., Pondard, N., McVerry, G., Ristau, J., Stirling, M., Thomas, J., Uma, S.R. and Zhao, J. (2012), "The Mw 6.2 Christchurch earthquake of February 2011: preliminary report", *NZ. J. Geol. Geophys.*, **55**(1), 67-90.

Kelly, J.M., Skinner, R.I. and Heine, A.J. (1972), "Mechanisms of energy absorption in special devices for use in earthquake resistant structures", *Bull. NZ. Nat'l Soc. Earthq. Eng.*, **5**(3), 63-88.

Kim, H.Y. and Atsumasa, O. (2005), "Surface deformations associated with the October 2004 Mid-Niigata earthquake: Description and discussion", *Earth Planets Space*, **57**(11), 1093-1102.

Koike, Y., Yanaka, T., Usami, T., Ge, H.B., Oshita, S., Sagou, D. and Uno, Y. (2008), "An experimental on developing study on developing high-performance stiffened shear panel dampers", *J. Struct. Eng.*, JSCE, **54**A, 372-381. (in Japanese)

Lew, M., Naeim, F., Huang, S.C., Lam, H.K. and Carpenter, L.D. (2000), "Geotechnical and geological effects of the 21 September 1999 Chi-Chi earthquake, Taiwan", *Struct. Des. Tall Build.*, **9**(2), 89-106.

Li, R., Ge, H.B., Usami, T. and Shu, G.P. (2016), "A strain-based post-earthquake serviceability verification method for steel frame-typed bridge piers installed with seismic dampers", *J. Earthq. Eng.*, **21**(4), 635-651.

Li, Y., Song, R. and van de Lindt, J. (2014), "Collapse fragility of steel structures subjected to earthquake mainshock-aftershock sequences", *J. Struct. Eng.*, ASCE, **140**(12), 04014095-1-10.

Lu, Z.H., Ge. H.B. and Usami, T. (2004), "Applicability of pushover analysis-based seismic performance evaluation procedure for steel arch bridge", *Eng. Struct.*, **26**(13), 1957-

1977.
Luo, X.Q., Ge, H.B. and Usami, T. (2009), "Parametric study on damage control design of SMA dampers in frame-typed steel piers", *Front. Archit. Civ. Eng*., **3**(4), 384-394.
Morishita, K., Usami, T., Banno, T. and Takahashi, M. (2002), "Applicability on dynamic verification method for seismic design of steel structures", *J. Struct. Eng*., JSCE, **48**A, 779-788.
National Research Institute for Earth Science and Disaster Prevention (NIED) (2004), 2004 Mid Niigata Earthquake, http://www.hinet.bosai.go.jp/topics/niigata_041023/?LANG=en&m=summary
Pan, K.Y., Wu, A.C., Tsai, K.Y., Li, C.H., Lin P.C., Wang, K.J. and Yang, C.S. (2016), "Seismic performance of reinforced concrete frames strengthened with buckling-restrained bracing steel frames", *Prog. Steel Build. Struct.*, **18**(1), 29-36.
Parker, M. and Steenkamp, D. (2012), "The economic impact of the Canterbury earthquakes", *Reserve Bank NZ. Bull.*, **75**(3), 13-25.
Potter, S.H., Becker, J.S., Johnston, D.M. and Possiter, K.P. (2015), "An overview of the impacts of the 2010-2011 Canterbury earthquakes", *Int. J. Disaster Risk Reduction*, **14**, 6-14.
Skinner, R.I., Kelly, J.M. and Heine, A.J. (1975), "Hysteresis damper for earthquake-resistant structures", *Earthq. Eng. Struct. D.*, **3**(3), 287-296.
Song, R., Li, Y. and van de Lindt, J. (2013), "Consideration of mainshock-aftershock sequences into performance-based seismic engineering", *Structures Congress 2013*, 2161-2167.
Tsai, K.C., Wu A.C., Wei, C.Y., Lin, P.C., Chuang, M.C. and Yu Y.J. (2014), "Welded end-slot connection and debonding layers for buckling-restrained braces", *Earthq. Eng. Struct. D.*, **43**(12), 1785-1807.
U.S. Geological Survey (USGS) (2011), Magnitude 9.0-near the east coast of Honshu, Japan, http://earthquake.usgs.gov/earthquakes/eqinthenews/2011/usc0001xgp/#summary.
Usami, T. (2002), "Fundamentals and applications for seismic design of steel bridges", (Subcommittee for Seismic Design of Steel Bridges, Task Committee of Performance-Based Seismic Design Methods for Steel Bridges, *Japan Society of Steel Construction* (JSSC)). (in Japanese)
Usami, T. (2002), "Seismic performance evaluation procedures and upgrading measures for steel bridges", (Subcommittee for Seismic Design of Steel Bridges, Task Committee of Performance-Based Seismic Design Methods for Steel Bridges, *Japan Society of Steel Construction* (JSSC)). (in Japanese)
Usami, T. (2006), "Seismic design guidelines for steel bridge", *Japan Society of Steel Construction* (JSSC).
Usami, T. and Ge, H.B. (2009), "A performance-based seismic design methodology for bridge systems" *J. Earthq. Tsunami*, **3**(3), 175-193.
Usami, T. and Sato, T. (2010), "Low-cycle fatigue tests and verification method for a steel buckling-restrained brace", *J. Struct. Eng.*, JSCE, **56**A, 486-498. (in Japanese)
Usami, T., Lu, Z.H., Ge, H.B. and Kono, T. (2004), "Seismic performance evaluation of steel arch bridge against major earthquakes. Part I: Dynamic analysis approach", *Earthq. Eng. Struct. D.*, **33**(14), 1337-1354.
Usami, T., Sato, T. and Kasai, A. (2009), "Developing high-performance buckling-restrained braces", *J. Struct. Eng.*, JSCE, **55**A, 719-729. (in Japanese)
Zheng, Y., Usami, T. and Ge, H.B. (2000), "Ductility of thin-walled steel box stub-columns", *J. Struct. Eng.*, ASCE, **126**(11), 1304-1311.